Origins of the diffuse shared proton vibrational signatures in proton-coupled electron transfer model dyad complexes

Cite as: J. Chem. Phys. 157, 154308 (2022); https://doi.org/10.1063/5.0122777

Submitted: 25 August 2022 • Accepted: 23 September 2022 • Accepted Manuscript Online: 26

September 2022 • Published Online: 21 October 2022

🗓 Liangyi Chen, Zifan Ma and 🗓 Joseph A. Fournier

COLLECTIONS

EP This paper was selected as an Editor's Pick







ARTICLES YOU MAY BE INTERESTED IN

Enhancing the signal strength of surface sensitive 2D IR spectroscopy
The Journal of Chemical Physics 150, 024707 (2019); https://doi.org/10.1063/1.5065511

CP2K: An electronic structure and molecular dynamics software package - Quickstep: Efficient and accurate electronic structure calculations

The Journal of Chemical Physics 152, 194103 (2020); https://doi.org/10.1063/5.0007045

Coupled local mode method for simulating vibrational spectroscopy

The Journal of Chemical Physics 157, 154103 (2022); https://doi.org/10.1063/5.0119631





Origins of the diffuse shared proton vibrational signatures in proton-coupled electron transfer model dyad complexes @

Cite as: J. Chem. Phys. 157, 154308 (2022); doi: 10.1063/5.0122777 Submitted: 25 August 2022 • Accepted: 23 September 2022 • **Published Online: 21 October 2022**







Liangyi Chen, D Zifan Ma, and Joseph A. Fournier D



AFFILIATIONS

Department of Chemistry, Washington University in St. Louis, St. Louis, Missouri 63130, USA

a) Author to whom correspondence should be addressed: jfournier@wustl.edu

ABSTRACT

Phenol-benzimidazole and phenol-pyridine dyad complexes have served as popular model systems for the study of proton-coupled electron transfer (PCET) kinetics in solution-phase experiments. Interpretation of measured PCET rates in terms of key structural parameters, such as the H-bond donor-acceptor distance, however, remains challenging. Herein, we report vibrational spectra in the electronic ground state for a series of phenol-benzimidazole and phenol-pyridine complexes isolated and cryogenically cooled in an ion trap. The four models studied each display highly red-shifted and broadened OH stretching transitions that arise from strong H-bonding interactions between the phenol OH group and the basic N site on benzimidazole/pyridine rings. The OH stretch transition in each model displays relatively strong absorption onsets near 2500 cm⁻¹ with broad shoulders that extend asymmetrically to higher frequencies over hundreds of wavenumbers. In contrast, the deuterated isotopologues yield much weaker OD stretch transitions that appear symmetrically broadened. The spectral breadth and shape of the OD stretch transitions are ascribed to variations in OD stretch frequencies that arise from zero-point distributions in the proton donor-acceptor low-frequency soft mode vibration. The asymmetric structure of the OH stretch transitions is attributed to a set of combination bands between the OH stretch and a series of low-frequency H-bond soft modes. The spectra and modeling highlight the importance of OH stretch-soft mode couplings, which are thought to play important roles in PCET and proton transfer dynamics.

Published under an exclusive license by AIP Publishing. https://doi.org/10.1063/5.0122777

I. INTRODUCTION

Proton-coupled electron transfer (PCET) reactions have long been known to drive pivotal biological processes¹⁻⁴ and are exploited in the design of catalysts for small-molecule activation^{5–10} organic synthesis. 11,12 Consequently, the development of quantitative models that accurately describe PCET reaction kinetics has been an important experimental and computational focus. 13-16 Experimentally, studies on model systems involving Tyr and/or His have been the most prevalent owing to the critical roles of these two amino acids as charge transfer mediators. ^{17–23} In particular, PCET involving the Tyrz-His₁₉₀ pair in photosystem II is a crucial component in the photosynthetic water oxidation cycle.^{24,25} In a series of papers, Hammarström and co-workers investigated phenol-benzimidazole and phenol-pyridine dyad complexes, which served as models for the Tyrz-His₁₉₀ pair.²⁶⁻²⁸ PCET was initiated by photoexciting the metal-to-ligand charge transfer transition

of Ru(bpy)₃²⁺, and reaction kinetics were measured by monitoring the recovery of the Ru(bpy)₃²⁺ ground state that resulted from electron transfer from the phenol group. The proton transfer component was then inferred through kinetic isotope effects and temperature-dependent measurements. The key goal of these studies was to correlate the measured PCET kinetics with the $O{\cdots}N$ proton donor-acceptor distances. While it was observed that PCET kinetics generally increased with decreasing proton donor-acceptor distance, quantitative modeling of the data remained difficult. In particular, simulations revealed a large distribution of O···N distances within the dyad systems due to low-frequency H-bond soft mode motions along the proton donor-acceptor coordinate.²⁸ Such motions are known to play a key role in enhancing proton transfer tunneling rates,^{2,28–33} but modeling the influence of these soft mode motions on PCET rates in the dyad systems was unsatisfactory. Questions regarding the role of electron conjugation effects in the tethered aromatic dyads were also raised.

A clear need still exists to interrogate PCET model systems in a more controlled and systematic fashion with a larger emphasis placed on directly monitoring the proton transfer coordinate. Recently, we have reported the cryogenic ion vibrational spectrum of a phenol-benzimidazole dyad complex [model (1) in Fig. 1] in the ground electronic state.³⁴ The strong cyclic OH···N intramolecular H-bond manifested in a highly red-shifted (2350 cm⁻¹ maximum) and broad (>1000 cm⁻¹) OH stretch transition even under the cryogenic conditions (28 K) of the experiments. Anharmonic calculations predicted relatively large cubic coupling constants between the OH stretch and a multitude of dark background doorway states deriving from combination bands and overtones involving fingerprint modes containing OH bend character. These predictions suggested that OH stretch-bend Fermi resonance interactions could be playing a key role in the observed spectral breadth. The full breadth of the OH stretch band could not, however, be completely accounted for through Fermi resonance interactions alone. Surprisingly, the OD stretch spectrum of the deuterated isotopologue likewise revealed a broad (~300 cm⁻¹) transition despite predictions of minimal Fermi resonance interactions within the OD stretch region. We hypothesized that the breadth of the OD stretch transition derived from the variation of the OD stretch frequency arising from zero-point displacements of H-bond soft modes along the proton transfer coordinate (formally H-atom transfer in electronic ground state models). The OH stretch spectrum was then rationalized in terms of an interplay between these soft mode displacements,

FIG. 1. Model dyad systems (1)–(4) characterized in this report.

which vary the OH stretch frequency, and Fermi resonance mode mixing.

In this report, we expand upon our previous study by investigating three additional dyad models, shown in Fig. 1 and hereafter referred to as (1)-(4), and more quantitatively unravel the origins of their diffuse H-bonded OH and OD stretch vibrational signatures. While key differences are observed between the vibrational spectra, each model displays similar OH and OD stretch patterns: the OH stretches show relatively strong absorption onsets that extend asymmetrically to higher frequencies, while the OD stretches are relatively weak and symmetrically broadened. The OD stretch spectra are accounted for by computing the variations of the OD stretch frequencies as a function of zero-point displacements of the lowestfrequency soft mode along the O···N H-atom transfer coordinate. The asymmetry and breadth of the OH stretch transitions are shown to derive from OH + soft mode combination bands using a model, which accounts for cubic coupling between the OH stretch and several quanta in a series of low-frequency modes. Stretch-bend Fermi resonance interactions play a smaller role than originally thought. Variations in OH and OD stretch transitions between the models are attributed to subtle differences in the soft mode frequencies and overall electronic structure of the dyad systems. Our results demonstrate the importance of low-frequency soft mode motions along the proton transfer coordinate on the vibrational spectra of PCET model systems and highlight the necessity of directly interrogating the proton transfer coordinate to better unravel the complexity of PCET reaction kinetics.

II. EXPERIMENTAL DETAILS

Model compounds (1)-(4) were synthesized according to literature protocols.²⁶ Details of the synthetic protocols are provided in the supplementary material. The spectroscopic experiments were carried out in a home-built photofragmentation mass spectrometer described in detail previously. Briefly, ions were produced from samples of ~200 μ M concentrations in methanol with trace amount of formic acid via electrospray ionization (ESI). Deuterium exchange of the labile protons was accomplished by saturating the ESI source region with D₂O vapor and purging with dry compressed air. The generated ions were guided through three differentially pumped vacuum chambers with RF hexapole ion guides into a 3D quadruple Paul trap attached to a closed-cycle helium cryostat held at 28 K. Buffer gas consisting of helium and a natural impurity of trace nitrogen was introduced into the trap through a pulsed valve. The ions were thermalized in the trap via collision with helium, leading to condensation of weakly bound N2 tag molecules onto the parent ions. Conditions were optimized for the condensation of a single N₂ molecule. Untagged ions were removed from the trap by a low amplitude RF pulse applied to the entrance trap electrode and modulated at the ions' secular frequency.

Following mass isolation, photofragmentation of the weakly bound N_2 adduct was induced through excitation with an optical parametric oscillator/amplifier (OPO/OPA) IR system (LaserVision) pumped by a Nd:YAG laser (Continuum Surelite EX, 10 Hz, 7 ns, 660 mJ/pulse). The resulting light was tunable from 2000 to 4500 cm⁻¹ with pulse energies ranging between 2 and 40 mJ depending on the frequency and bandwidth of ~3 cm⁻¹. Difference-frequency mixing of the OPA signal and idler beams in AgGaSe₂

extended the output range into the $600-2200~{\rm cm}^{-1}$ fingerprint region with $\sim 1~{\rm mJ}$ pulse energies. The IR light was focused directly into the ion trap with a spherical mirror through a KBr window.

Ions were extracted from the trap into a reflectron time-of-flight mass spectrometer (Jordan TOF Products, Inc.) by pulsing the exit electrode of the ion trap to -400 V. A dual-stage reflectron focused the ions onto a dual MCP detector. The tag-loss photofragmentation signal was recorded as a function of the scanned laser frequency to obtain linear action spectra. Spectra were normalized by the laser power to take into account large variations in laser power over the scanning range. Spectra in the higher-frequency region were collected at reduced laser powers to ensure linearity. The reported spectra were averages of ~ 20 scans binned by 1 cm $^{-1}$.

III. COMPUTATIONAL DETAILS

Quantum chemical calculations were performed at the B3LYP/ 6-311+G(d,p) level of theory and basis set in Gaussian09. Harmonic spectra in the high-frequency region ($2000\text{-}3700~\text{cm}^{-1}$) were scaled by a common factor of 0.968 for each model, which brought the predicted NH stretches into close agreement with experimental positions. In the lower-frequency region ($1200\text{-}2100~\text{cm}^{-1}$), a scaling factor of 0.983 was used for each model to bring the highest-energy transitions near $1600~\text{cm}^{-1}$ into close agreement with those observed.

The dependencies of OH and OD stretch frequencies on displacements in the lowest-frequency soft mode along the H-atom transfer coordinate were determined by calculating OH/OD stretch frequencies at geometries spanning the classical turning points along the normal mode coordinate at the zero-point level. Only the shared proton was allowed to relax in these calculations. A total spectrum was constructed by convolving the predicted OH/OD stretch spectra at each geometry weighted by the corresponding probability density at the zero-point level. Further details about the approach are provided in the supplementary material.

To determine the degree of coupling between the OH stretches and low-frequency soft modes, which give rise to OH + soft mode combination bands, matrix elements of the following vibrational Hamiltonian were computed and diagonalized in a similar approach to that recently reported by Craig *et al.*:³⁷

$$H = \left(\nu_{OH} + \frac{1}{\sqrt{8}} \sum_{s} F_{OH,OH,s} \left(a_{s}^{+} + a_{s}^{-}\right)\right) \left(\hat{n}_{OH} + \frac{1}{2}\right) + \sum_{s} \nu_{s} \hat{n}_{s}. \eqno(1)$$

Here, the subscript "s" refers to the low-frequency soft modes included in the model, $F_{OH,OH,s}$ are the cubic coupling constants from anharmonic second-order vibrational perturbation theory (VPT2) calculations, \hat{n} is the number operator, and a_s^{\pm} denote the harmonic oscillator raising/lowering operators for the soft modes.

The Hamiltonian matrix H can be computed from Eq. (1) for the OH fundamental and its combination bands involving N soft modes, v_s^N . The diagonal elements are the energies of all states included, i.e., the OH fundamental and the OH + soft mode combination bands. The energy of the combinations bands is given by

$$E = v_{OH} + \sum_{i=1}^{N} n_i v_s^i,$$
 (2)

where n_i is the number of quanta in soft mode i. Up to 2000 cm⁻¹ of energy distributed among the soft modes were considered such that

$$\sum_{i=1}^{N} n_i v_s^i < 2000 \text{ cm}^{-1}.$$
The off-diagonal elements

The off-diagonal elements of H are calculated using the cubic coupling constants $F_{OH,OH,s}$ between the OH stretch and OH + soft mode combination bands. By expanding the Hamiltonian in Eq. (1), one can find that the matrix elements are non-zero if and only if one of the included soft mode energies differs by one level. That is,

$$H = \langle 1, m_1, m_2, m_3, ..., m_N | \hat{H} | 1, n_1, n_2, n_3, ..., n_N \rangle$$

$$= \begin{cases} \frac{3j}{4\sqrt{2}} F_{OH,OH,i} \text{ when } \sum_{i=1}^{N} |m_i - n_i| = |m_j - n_j| = 1, \\ 0 \text{ when } \sum_{i=1}^{N} |m_i - n_i| \neq 1. \end{cases}$$
 (3)

Further details of the derivation are provided in the supplementary material.

IV. RESULTS AND DISCUSSION

A. Computed structures and predicted OH stretch frequencies

Unscaled harmonic and anharmonic VPT2 frequencies for the H-bonded OH stretch in the four model systems are summarized in Table I along with the critical O···N H-atom donor-acceptor distance, d_{ON}. The relatively short d_{ON} values (~2.54 Å) predicted for each model suggest that strong H-bonding interaction should be anticipated, although the OH···N H-bond angles of ~149° deviate significantly from the ideal linear scenario. The calculated harmonic OH stretch frequencies range from 2800 to 2900 cm⁻¹ and, as expected for unscaled results, fall much higher in frequency than the observed vibrational signatures discussed below. The anharmonic VPT2 predictions, on the other hand, appear to overestimate the strengths of the H-bonds and place the OH stretches in the 2100-2400 cm⁻¹ range. The ordering of the OH stretch frequencies, (1) < (4) < (3) < (2), roughly correlates with d_{ON} in accordance with Badger's rule.³⁸ The exception is between models (1) and (4), where (4) is predicted to have a slightly shorter don but a slightly higher OH stretch frequency. This discrepancy, along with the large variations predicted between (1) and (2), suggests that the tert-butyl group adjacent to the phenol OH in (1) has a significant impact on the electronic structure. We explore this further below. We note that, although the basicity of benzimidazole is slightly greater than that of

TABLE I. Calculated OH stretch vibrational frequencies and H-bond structural parameters for the model systems. Calculations were performed at the B3LYP/6-311+G(d,p) level and basis set. Anharmonic VPT2 frequencies are in parentheses. All vibrational frequencies are unscaled.

| Model | $\mathbf{v}_{\mathrm{OH}}~(\mathrm{cm}^{-1})$ | d _{ON} (Å) | d _{OH} (Å) | ∠OHN (deg) |
|-------|---|---------------------|---------------------|------------|
| 1 | 2811 (2111) | 2.534 | 1.014 | 149.5 |
| 2 | 2920 (2409) | 2.559 | 1.010 | 147.6 |
| 3 | 2857 (2197) | 2.536 | 1.013 | 148.9 |
| 4 | 2826 (2126) | 2.533 | 1.015 | 149.1 |

TABLE II. Systematic variations in the calculated OH stretch frequencies and H-bond structural parameters for several substituted phenol-benzimidazole dyads. Calculations were performed at the B3LYP/6-311+G(d,p) level and basis set. Harmonic vibrational frequencies are unscaled. Entries are listed by increasing d_{ON} values.

pyridine, the larger bond angles in the six-membered pyridine ring result in a shorter $d_{\rm ON}$ value.

Given the subtle differences in structure and questions regarding the impact of electron conjugation effects on these model dyads, we computationally explored the structural and OH stretch frequency variations on the phenol-benzimidazole dyad shown in Table II by systematically varying the substituents in the paraposition (R_1) and *ortho*-position (R_2) relative to the hydroxyl group. Interestingly, the neutral dyad with $R_1 = R_2 = H$ is predicted to have a much longer d_{ON} and, consequently, an OH stretch frequency that lies over 300 cm⁻¹ higher than that computed for (2). We first investigated the influence of the excess proton by substituting $R_1 = NH_3^+$. The resulting d_{ON} and OH stretch frequencies nearly match those predicted for (2). The presence of the excess charge clearly has a significant influence on the electronic structure and H-atom transfer coordinate, likely due to delocalization of the positive charge via conjugation effects within the aromatic dvad system. Indeed, substituting $R_1 = CH_2NH_3^+$ to break resonance sharing does blueshift the predicted OH stretch but by only 25 cm⁻¹ compared to R₁ = NH₃⁺. Adding a second CH₂ linker (R₁ = CH₂CH₂NH₃⁺) further blue-shifts the OH stretch; however, its frequency still remains >100 cm⁻¹ lower than in the neutral dyad. Considerable charge sharing and delocalization, therefore, persist even when the excess proton is relatively remote from the dyad core.

To further quantify the influence of conjugation effects, we substituted R_1 = benzimidazole to give the neutral precursor of (2). The additional aromatic ring slightly perturbs the structure and results in a small OH stretch red-shift of ~40 cm⁻¹ compared to the simpler neutral model ($R_1 = R_2 = H$). Protonation of benzimidazole in the R_1 position to give (2) then results in a much shorter d_{ON} and lower OH stretch frequency. While conjugation effects in neutral systems do increase the H-bond strength slightly (pK_a of phenol is ~10, while that of *para*-phenylphenol is ~9.5), the presence of the excess proton

causes a more significant perturbation in the structure. Protonated para-substituted groups appear to act as strong electron withdrawers, increasing the acidity of the phenol OH and resulting in shorter $d_{\rm ON}$ values. To corroborate this conclusion, we include results from substituting neutral electron withdrawing groups $R_1 = NO_2$ and $R_1 = CN$. Both substituents result in a shortening of $d_{\rm ON}$ and redshift of the OH stretch compared to $R_1 = H$, but to a lesser extent compared to the protonated substituents.

We next turn to the effects of substituting a *tert*-butyl group in the R₂ position ortho to the hydroxyl group. Substituting tert-butyl into the simplest model ($R_1 = H, R_2 = tert$ -butyl) decreases d_{ON} by 0.03 Å and results in a nearly 100 cm⁻¹ red-shift in the OH stretch. The shortest d_{ON} and lowest OH stretch frequencies are predicted for tert-butyl substituted charged models (R₁ = NH₃⁺ or benzimidiazoleH⁺, R₂ = tert-butyl). Although tert-butyl is an electron donating group that nominally causes a decrease in acidity, the perturbations induced by steric hindrance in the *ortho*-position increases the acidity of the phenolic OH (the "ortho" effect^{39–41}). Therefore, the combination of electron conjugation, protonation, and the ortho effect makes phenolic OH in (1) the most acidic among the studied models and yields the strongest intramolecular H-bond. We also include the results for R_2 = methyl and R_2 = isopropyl in Table II. While the effects of these two groups are smaller compared to tert-butyl, the calculations show a clear trend of don decreasing and OH stretch red-shifting with the increasing bulkiness of the R2 substituent.

B. Survey of cryogenic ion vibrational spectra

1. OH stretch region

The higher-energy 2000–3700 cm⁻¹ region of the IR spectra for the four model systems is shown in Fig. 2. Harmonic calculations for this region are represented in Fig. S1of the supplementary material,

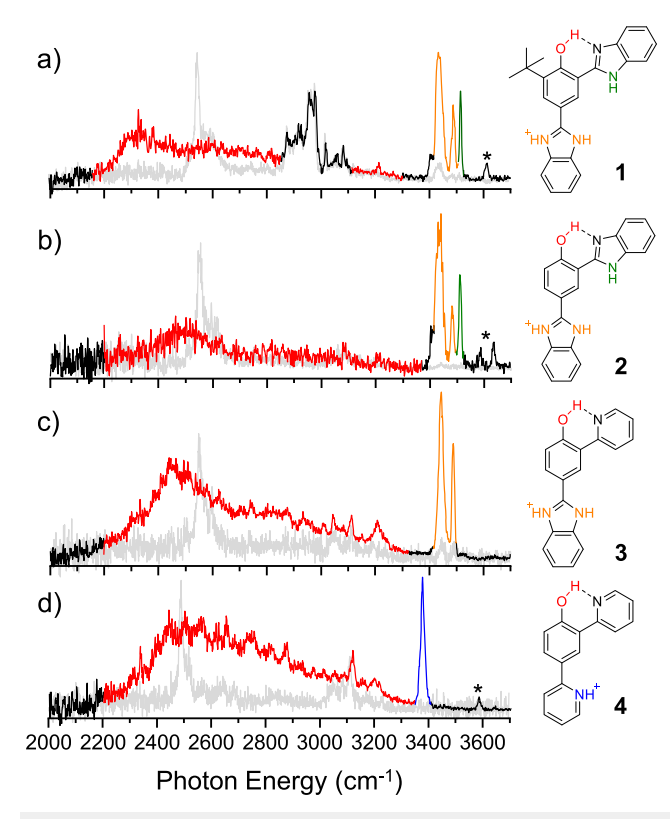


FIG. 2. Cryogenic ion vibrational spectra in the OH and NH stretch region. (a) Model **(1)**. (b) Model **(2)**. (c) Model **(3)**. (d) Model **(4)**. Red: H-bonded OH stretch. Orange: *para*-benzimidazoleH⁺ NH stretches. Green: *ortho*-benzimidazole NH stretch. Blue: *para*-pyridineH⁺ NH stretch. The weak transitions labeled with asterisks near 3600 cm⁻¹ are due to isomers where there is a non-H-bonded OH stretch. The spectra in gray are from isotopologues where the labile protons are exchanged for deuterons.

but the relatively simple band patterns allow for direct assignments by inspection. The highest-energy transition near 3500 cm⁻¹ (colored green) observed in (1) and (2) derives from the *ortho*-benzimidazole NH stretch. The pair of transitions at 3440 and 3485 cm⁻¹ (colored orange) seen in (1)–(3) derives from the two NH⁺ stretches on the protonated *para*-benzimidazoleH⁺ group. The strong transition at 3370 cm⁻¹ in (4) derives from the NH⁺ stretch of the protonated *para*-pyridineH⁺ ring in that model. The series of intense sharp bands spanning 2900–3000 cm⁻¹ in (1) results from the various CH stretching modes of the *tert*-butyl group. The aromatic CH stretches in the 3000–3200 cm⁻¹ range are predicted to be much weaker, but can be more readily identified in the deuterated spectra (gray background traces in Fig. 2).

The most prominent feature in each spectrum is the broad transition (red) that arises from the strong intramolecular $OH \cdots N$ H-bond. The weak transitions near 3600 cm⁻¹ (denoted by asterisks in Fig. 2) observed in (1), (2), and (4) result from a population of isomers where the OH stretch is non-H-bonded. We showed in our previous study that the *ortho* N-containing ring can become protonated during the ionization process, which subsequently breaks the intramolecular $OH \cdots N$ H-bond.³⁴ Formation of the $OH \cdots N$

H-bond in the dominant isomer, therefore, results in $\sim 1000~\rm cm^{-1}$ red-shift of the phenolic OH stretch. Models (1)–(3) show similar patterns: a strong, distinct onset of the absorption followed by an asymmetric tail with a secondary "hump" of about 300– $400~\rm cm^{-1}$ higher than the initial maximum. The OH stretch transition in (4) appears more congested throughout the band profile compared to the other models. The OH stretch transition in each model spans $\sim 1000~\rm cm^{-1}$, and the sharper substructure within the bands is apparent. The absorption onset is lowest in frequency in (1) and highest in (2), consistent with the predicted $d_{\rm ON}$ values and H-bond strengths.

2. Fingerprint and OD stretch region

The lower-energy 1200–2100 cm⁻¹ spectral region of the deuterated model systems is represented in Fig. 3 along with the corresponding harmonic predictions. The experimental spectra of the light isotopologues are shown in gray for comparison, and the corresponding harmonic calculations are given in Figs. S2–S5. The

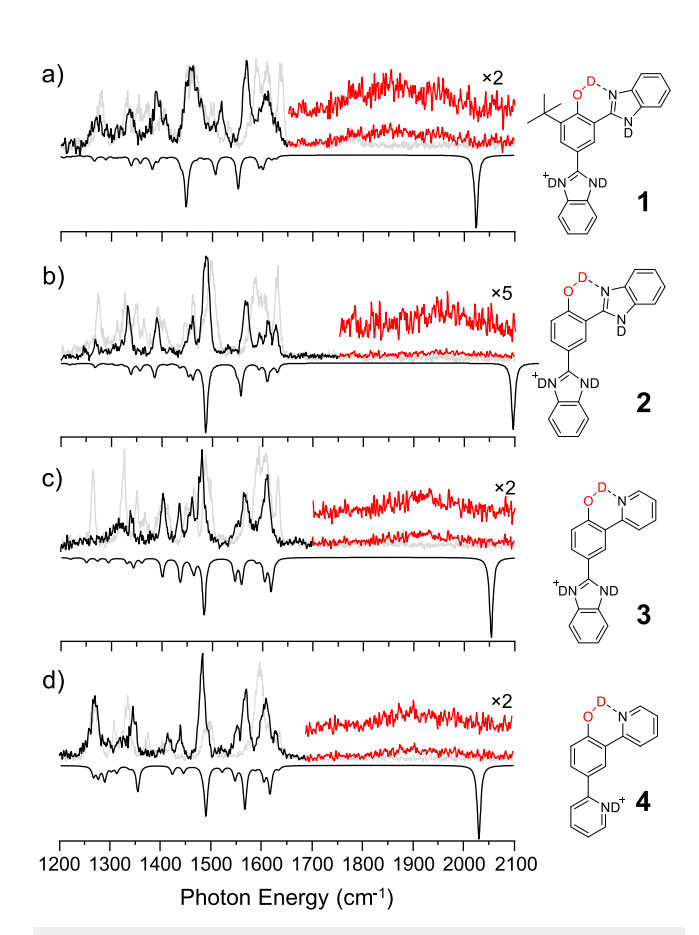


FIG. 3. Cryogenic ion vibrational spectra of the deuterated isotopologues in the fingerprint region. (a) Model **(1)**. (b) Model **(2)**. (c) Model **(3)**. (d) Model **(4)**. Spectra of the light isotopologues are shown in gray. Scaled (0.983) harmonic predictions for the deuterated models are given by the inverted traces. The broad OD stretches centered near 1900 cm⁻¹ for each model are highlighted in red. Assignments for the lower-energy transitions for both isotopologues are provided in the supplementary material.

calculated harmonic spectra for each model yield excellent agreement with the experimental spectra in the congested fingerprint region. Many of these transitions are predicted to have complicated normal mode displacements that involve NH and OH bending motions, which is evidenced by the extent of spectral shifting upon deuteration of the labile NH and OH protons. Specific assignments and normal mode displacement vectors of the strongest transitions are provided in Figs. S2–S5.

The key features of interest in the deuterated isotopologues are the OD stretches. The scaled harmonic calculations predict the OD stretch transitions to occur in the 2000–2100 cm $^{-1}$ range with intensities about half that of the OH stretches. The anharmonic VPT2 calculations again overestimate the H-bond strengths with unscaled OD stretch frequencies predicted to occur in the 1700–1800 cm $^{-1}$ range. Relatively weak transitions are observed near 1900 cm $^{-1}$ that are 200–300 cm $^{-1}$ broad for each model and are absent in the light isotopologues. These features, therefore, are assigned to the OD stretches. In contrast to the OH stretches, the OD stretches appear symmetrically broadened about the absorption maxima. The frequencies of the OD stretch maxima, (1) < (4) < (3) < (2), track with the predicted H-bond strengths and those inferred from the experimental OH stretch onset bands.

C. H-bond soft mode displacements and breadth of the OD stretches

To quantify the effects of zero-point displacements in H-bond soft modes, 42,43 we computed the OH and OD stretch frequencies at geometries that span the classical turning points at the zero-point level of the lowest-frequency normal mode which significantly varies the O···N distance. These low-frequency normal modes, shown in Fig. 4, have frequencies of ~90 cm $^{-1}$ [model (1)], $115~{\rm cm}^{-1}$ [model (2)], and $170~{\rm cm}^{-1}$ [models (3) and (4)]. The $d_{\rm ON}$ values span nearly 0.1 Å for each model and result in a frequency range of ~300 cm $^{-1}$ for the OH stretches within the classical turning points (Fig. 4). There is also a nearly linear correlation between $d_{\rm ON}$ and OH stretch frequency. The corresponding results for the OD stretches are represented in Fig. S6 and predict ~200 cm $^{-1}$ deviations in the OD stretch frequencies.

Figures 5(a)-5(d) compare the experimental OD stretch transitions to the convolution of the probability density-weighted OD stretch frequencies accessible within the classical turning points of the low-frequency soft modes identified in Fig. 4. The approach provides excellent agreement with the experimental spectral breadth of the OD stretches for each dyad. In addition, we predicted Fermi resonance coupling between the OD stretch and background doorway

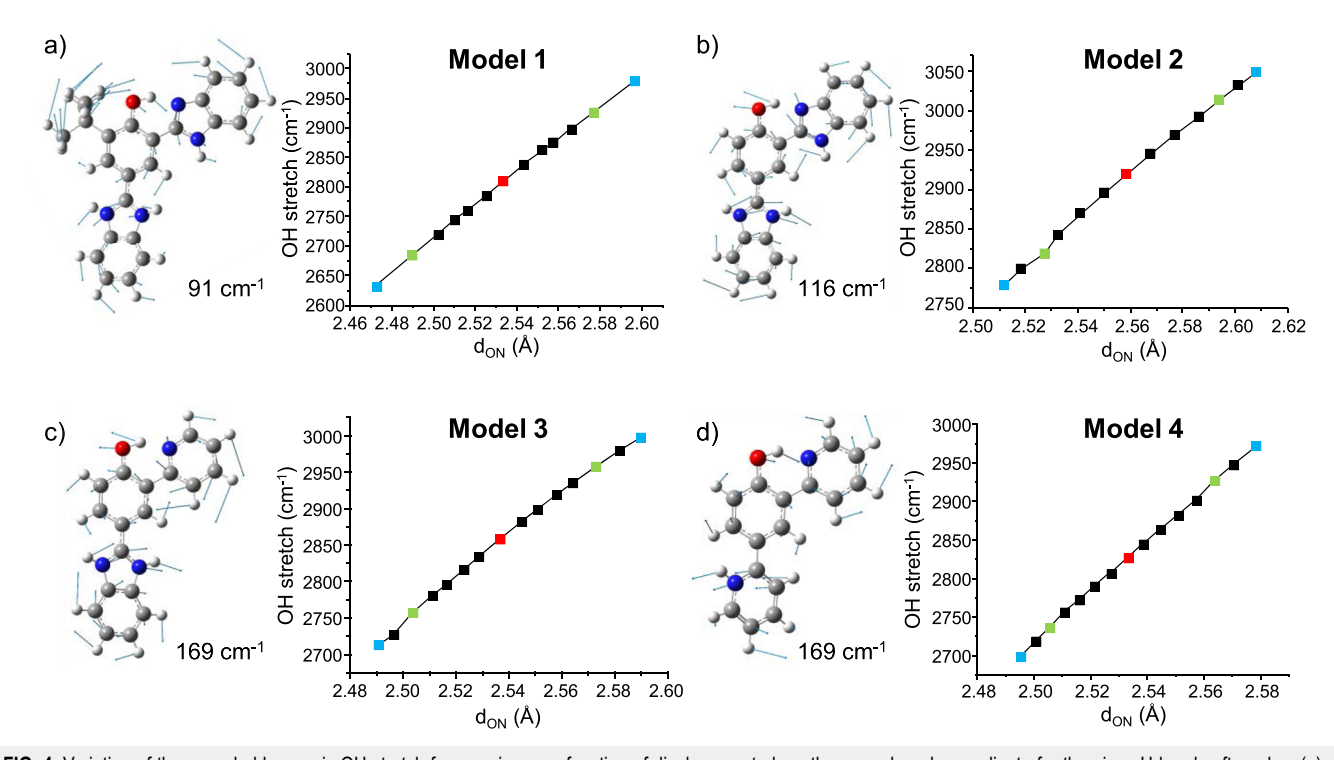


FIG. 4. Variation of the unscaled harmonic OH stretch frequencies as a function of displacement along the normal mode coordinate for the given H-bond soft modes. (a) Model (1). (b) Model (2). (c) Model (3). (d) Model (4). Red boxes represent the minimum-energy structures. Blue boxes represent the classical turning points at the zero-point level. Green boxes represent the zero-point level root mean square displacements.

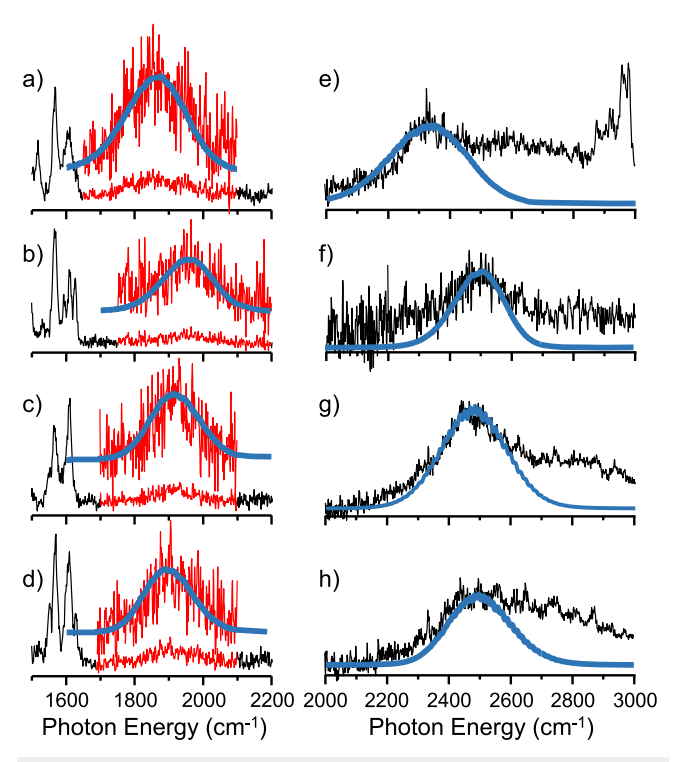


FIG. 5. (a)–(d) Comparison of the experimental OD stretch region (red) with the predicted distribution of OD stretch frequencies (blue) expected from zero-point displacements along the low-frequency H-bond soft modes identified in Fig. 4. (e)–(h). Analogous OH stretch distributions compared to the experimental spectra for each dyad.

states involving OD bending modes using computed VPT2 cubic coupling constants⁴⁴ (Fig. S7). While modest mode coupling is predicted, Fermi resonance coupling between background states and the OD stretch at a single frequency does not account for the full breadth of the OD stretch transitions. The results suggest, however, that Fermi resonance interactions likely contribute to the observed substructure within the band envelopes. Although it is a simplified computational approach, the good agreement with the experimental spectra demonstrates that zero-point soft mode displacements along the H-atom transfer coordinate adequately capture the underlying mechanics driving the breadth of the OD stretch transitions.

Figures 5(e)-5(h) show the analogous distributions of the OH stretch frequencies compared to the experimental spectra of each dyad. The predicted distributions reasonably reproduce the breadths of the dominant low-frequency absorption onset bands. The high-frequency asymmetric tails of the OH stretch transitions, however, are not captured by this approach.

D. Soft mode coupling and asymmetry of the OH stretch transitions

To better understand the origins of the OH stretch asymmetry, we first consider the role of Fermi resonance interactions. The anharmonic VPT2 calculations predict large (>50 cm⁻¹) cubic coupling constants between the OH stretches and overtones/combination bands deriving from fingerprint modes which

possess OH bend character. The highest density of these doorway states, however, occurs in the 2800-3200 cm⁻¹ range. As demonstrated in our previous study on (1), significant mode mixing and dilution of the OH stretch would be anticipated if the fundamental fell within this spectral region.³⁴ Figures 6(b) and 6(f) represent the predicted Fermi resonance coupling for models (1) and (3) for several OH stretch frequencies that span the distributions given in Fig. 5. The experimental spectra of (1) and (3) are reproduced in Figs. 6(a) and 6(e), respectively, for comparison. The amount of mode mixing predicted is quite minimal, given the highly red-shifted origins of the OH stretch fundamentals. Like the OD stretches, Fermi resonances likely contribute to the breadth and substructure within the OH stretch onset region. The distribution of OH stretch frequencies accessible due to low-frequency soft mode displacements, however, is not sufficient to "turn on" the stronger Fermi resonance interactions expected at higher frequencies. Fermi resonances, therefore, do not appear to play a role in the asymmetry of the OH stretches. Results for the other two models are provided in Fig. S8.

We next consider cubic coupling between the OH stretches and the low-frequency soft modes identified in Fig. 4. In the CH₃NO₂-·H₂O and CH₃CO₂-·H₂O cluster systems, strong Franck-Condon-like progressions were observed in the water stretching region with spacings consistent with the low-frequency rocking motion of the H-bonded water molecule. 45,46 Adiabatic modeling showed that excitation of the OH stretches results in a strengthening of the anion-water H-bond interaction, causing a shift in the low-frequency water rocking soft mode potential energy surface that leads to the observed Franck-Condon progressions. The progression patterns can be predicted through intensity sharing of the OH stretch to OH + soft mode combination bands using calculated anharmonic cubic coupling constants. 47,48 The anharmonic VPT2 calculations on the dyads predict cubic coupling constants in the range of 125-155 cm⁻¹ between each respective OH stretch and its combination band with the low-frequency soft modes identified in Fig. 4. The predicted Franck-Condon progressions for (1) and (3) are shown in Figs. 6(c) and 6(h). Those for the other two models are included in Fig. S8. Excitation out to four quanta in the soft mode is predicted for (1), while the predicted spectrum for (3) is dominated by the origin band. This difference is due to the lower soft mode frequency in (1) compared to (3). Although a soft mode progression could partially explain the high-frequency asymmetry, the predicted progressions from a single soft mode do not satisfactorily account for the full breadth of the OH stretch regions.

In addition to the soft modes identified in Fig. 4, the VPT2 calculations predict large cubic coupling constants between the OH stretches and numerous additional soft modes with vibrational frequencies spanning $60-600~\rm cm^{-1}$ that display significant displacements in the O···N coordinate. A recent cryogenic ion spectroscopic study of the hydronium ion trapped in 18-crown-6 ether by Craig et al. 37 revealed a broad H-bonded hydronium OH stretch with an asymmetric line shape quite similar to those observed in the dyads reported here. An extended adiabatic model that included cubic couplings between the hydronium OH stretches and the four lowest-frequency soft modes which displaces the embedded hydronium ion within the crown ether was used to rationalize the breadth and asymmetry of the OH stretch feature.

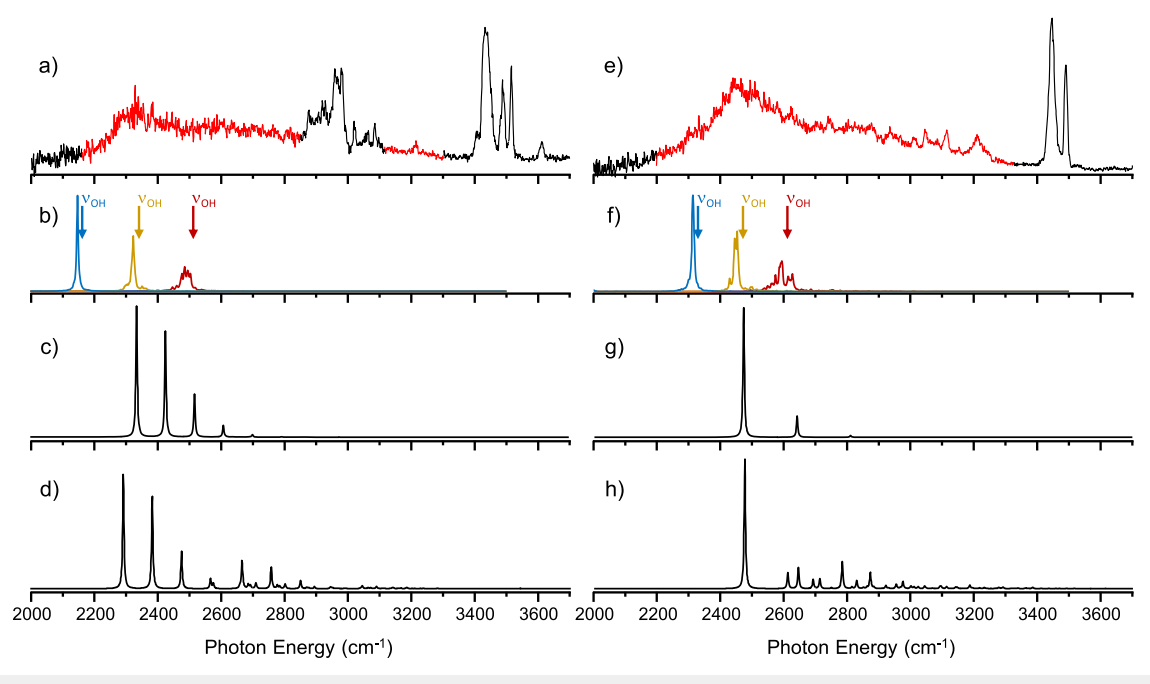


FIG. 6. OH stretch region of (a) model **(1)** and (e) model **(3)** reproduced from Fig. 2. (b) and (f) Predicted transitions from Fermi resonance coupling between the OH stretch and background doorway states for three different OH stretch frequencies indicated by the colored arrows. (c) and (g) Predicted progressions of OH + soft mode combination bands calculated using anharmonic VPT2 cubic coupling constants. Only the respective soft modes identified in Fig. 4 are included. (d) and (h) Predicted spectra for coupling of the OH stretch to several low-frequency soft modes along the H-atom transfer coordinate.

We employed the same extended model on the dyad systems that includes coupling to 6–10 soft modes whose vibrational frequencies fall below 500 cm⁻¹ and have predicted cubic coupling constants in the 50–300 cm⁻¹ range. The specific soft mode frequencies and cubic coupling constants for each dyad are reported in the supplementary material. The results for (1) and (3) are represented in Figs. 6(d) and 6(h) and are also reproduced in Fig. 7 along with those for (2) and (4). The model predicts a series of transitions 200–600 cm⁻¹ higher in vibrational frequency than the OH stretch origin band that reasonably captures the frequency position and spectral extent of the observed asymmetric shoulders for each dyad. Indeed, the largest cubic coupling constants predicted by VPT2 are between the OH stretches and the soft modes that have frequencies in the 300–400 cm⁻¹ range.

While the extended soft mode coupling model rationally explains the origins of the broad and asymmetric OH stretch transitions, the density of transitions predicted does not fully account for the highly congested and continuous nature of the OH transition profiles. For the OH stretch origin band, further dilution is anticipated from Fermi resonance interactions and broadening from the same zero-point soft mode distributions that drives the breadth of the OD stretches [Figs. 5(b) and 5(f)]. Furthermore, we posit that additional spectral broadening likely results from ultrafast relaxation of the excited OH stretches. In the HCO2⁻·H₂O cluster anion, Hamm and Stock identified vibrational conical intersections between the water OH stretch and HOH bend overtone surfaces, which promote fast relaxation of the OH stretch.⁴⁹ Dephasing times

of ~400 fs accounted for the observed spectral breadth in that system. Yang et al. presented line shape analyses of the water OH stretches in the Cs⁺(H₂O)₂₀ cluster that suggested dephasing times as fast as 75 fs for the most strongly H-bonded oscillators.⁵⁰ A recent theoretical analysis of the strong NH···O H-bond in electronically excited methyl anthranilate by Sibert et al. predicted an NH stretch lifetime of ~40 fs.⁵¹ Very closely related to the model dyads studied here, Balasubramanian et al. measured solution-phase transient absorption IR spectra of the phenol-benzothiazole dyad, which revealed ultrafast relaxation of the OH stretch within 100 fs.⁵² Excitingly, these measurements also revealed periodic oscillations in the OH stretch ground-state bleach signals corresponding to coherent coupling with several soft modes spanning 100-250 cm⁻¹, quite similar to those considered in the extended coupling model employed here. Figure 7 includes the predicted band profiles if 50 cm⁻¹ of bandwidth are added to each transition, corresponding to modest ~200 fs dephasing times for the OH stretches. This added broadening more accurately captures the total breadth and shape of the transition profiles. More sophisticated calculations that include higher-order anharmonic effects^{53,54} and rigorous relaxation dynamics⁴ likely necessary to better reproduce the spectral profiles.

The predicted and observed differences between the four dyads arise from differences in the number of soft modes that displace the $O \cdot \cdot \cdot N$ coordinate and their frequencies. The structural perturbations induced by the *tert*-butyl group in (1) result in the lowest frequency in-plane soft mode and generally larger cubic coupling constants overall. The notable differences between (3) and (4) are

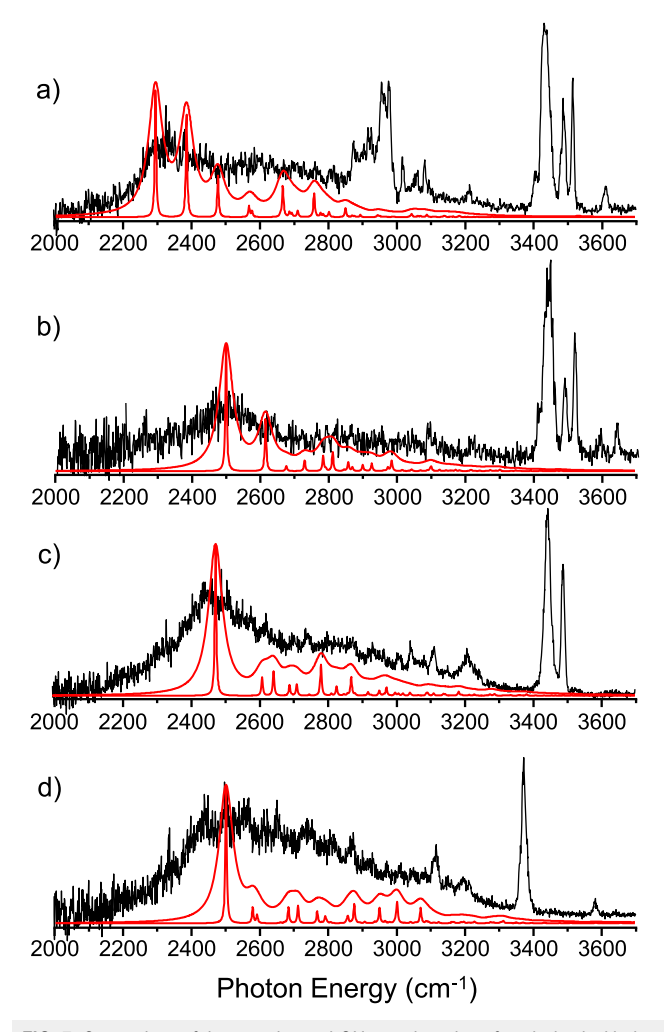


FIG. 7. Comparison of the experimental OH stretch region of each dyad with the anharmonic spectra predicted using the model Hamiltonian that couples the OH stretch to several low-frequency H-bond soft modes. (a) Model **(1)**. (b) Model **(2)**. (c) Model **(3)**. (d) Model **(4)**. Also shown are the predicted spectra when broadening the calculated transitions by 50 cm $^{-1}$ to account for ultrafast dephasing (\sim 200 fs) of the OH stretches.

more surprising, given that the only variation is the identity of the charged appended group in the para-position. Despite the appended charged group being seemingly remote from the $O\cdots N$ coordinate, its identity results in key subtle differences to the structure and vibrational spectrum (see Table 1). These subtle differences have profound effects on the low-frequency modes as (4) is predicted to have nearly a dozen soft modes with significant $O\cdots N$ displacement, including several very low frequency out-of-plane motions. The additional low-frequency modes in (4) appear responsible for the highly congested nature of its OH stretch spectrum.

Finally, we address the isotopic differences in the OH and OD stretch regions of the light and deuterated isotopologues. The symmetrically broadened OD stretches were adequately accounted for using the simple soft mode distribution model (Fig. 5) and show no clear evidence of the cubic soft mode coupling observed for the

OH stretches. The anharmonic VPT2 calculations on the deuterated dyads predict cubic coupling constants between the OD stretch and the same set of soft modes used in the extended coupling model that are ~1.4-times less than those for the light isotopologues, as expected. OD stretch-soft mode combination bands are still predicted using the extended coupling model for the deuterated species but are predicted to be weaker compared to the light isotopologues (Fig. S9). We suspect that OD stretch-soft mode combination bands are present but were too weak to observe within the signal-to-noise ratio, given the relatively weak OD stretch transitions, smaller coupling constants, and low laser power in this spectral region. We again note that the OD stretches are predicted to be about half as intense as the OH stretches at the harmonic level. The presence of OD stretch-soft mode coupling could further explain why the OD stretches appear to be quite weak. In any scenario, it is apparent that numerous broadening and anharmonic coupling mechanisms are at play in the hydron stretching regions in both sets of isotopologues.

V. SUMMARY

Cryogenic ion vibrational spectroscopy benzimidazole and phenol-pyridine PCET model complexes reveals strong H-bonding interactions between the proton donor-acceptor groups that manifest in broad OH and OD stretch transitions. Anharmonic modeling reveals a complicated interplay between Fermi resonance interactions, zero-point soft mode distributions, and cubic coupling to low-frequency modes which modulates the O···N H-atom transfer coordinate. Additional broadening is attributed to ultrafast relaxation of the strongly coupled OH stretches. Although the modeled spectra shown in Fig. 7 are not in exact quantitative agreement with the experimental spectra, they demonstrate that coupling between the OH stretch and several low-frequency soft modes is the most likely governing interaction, giving rise to the asymmetric line shapes and overall spectral extent.

Critically, soft mode motions along the proton transfer coordinate are known to play pivotal roles in proton transfer dynamics. The presented experimental spectra directly reveal the manifestation of soft mode coupling to the onset of intramolecular H-atom transfer in the dyad systems. Temperature-dependent studies that enable thermal excitation of the soft modes will provide further key experimental insights into the H-atom transfer surface and could provide access to the H-atom transfer product species. Although the proton transfer surface will be quite different in the electronic excited state during a PCET reaction, the soft mode motions along the O···N coordinate identified here will remain crucial components that dictate the reaction dynamics. Establishing the ground-state proton transfer surfaces and vibrational dynamics will provide a better starting point with which to unravel PCET dynamics and mechanisms.

SUPPLEMENTARY MATERIAL

See the supplementary material for synthetic protocols of dyad complexes; further details on anharmonic analyses and the summary of VPT2 results; harmonic predictions in the OH/NH stretch regions (Fig. S1); harmonic spectra of the light and deuterated

isotopologues in the fingerprint region (Figs. S2–S5); variation in the OD stretches with lowest-frequency soft mode displacement (Fig. S6); Fermi resonance analysis in the OD stretch region (Fig. S7); anharmonic modeling for dyads (2) and (4) (Fig. S8); and the extended soft mode cubic coupling model applied to the deuterated dyad species (Fig. S9).

ACKNOWLEDGMENTS

This work was supported by the National Science Foundation through a CAREER Award under Grant No. CHE-2044927 and Washington University in St. Louis. The authors thank Professors Anne McCoy and Ned Sibert for insightful discussions.

AUTHOR DECLARATIONS

Conflict of Interest

The authors have no conflicts to disclose.

Author Contributions

Liangyi Chen: Investigation (lead); Data curation (lead); Formal analysis (lead); Methodology (lead); Validation (equal); Visualization (lead); Writing – original draft (supporting); Writing – review and editing (supporting). Zifan Ma: Investigation (supporting); Formal analysis (supporting); Writing – review and editing (supporting). Joseph Fournier: Conceptualization (lead); Funding acquisition (lead); Methodology (supporting); Project administration (lead); Supervision (lead); Validation (equal); Visualization (supporting); Writing – original draft (lead); Writing – review and editing (lead).

DATA AVAILABILITY

The data that support the findings of this study are available from the corresponding author upon reasonable request.

REFERENCES

- ¹ M. Byrdin, S. Villette, A. Espagne, A. P. M. Eker, and K. Brettel, J. Phys. Chem. B 112, 6866 (2008).
- ²M. J. Knapp, K. Rickert, and J. P. Klinman, J. Am. Chem. Soc. **124**, 3865 (2002).
- ³ A.-F. Miller, K. Padmakumar, D. L. Sorkin, A. Karapetian, and C. K. Vance, J. Inorg. Biochem. **93**, 71 (2003).
- ⁴V. R. I. Kaila, M. P. Johansson, D. Sundholm, L. Laakkonen, and M. Wikström, Biochim. Biophys. Acta, Bioenerg. **1787**, 221 (2009).
- ⁵ A. Magnuson, P. Liebisch, J. Högblom, M. F. Anderlund, R. Lomoth, W. Meyer-Klaucke, M. Haumann, and H. Dau, J. Inorg. Biochem. **100**, 1234 (2006).
- ⁶M. F. Anderlund, J. Högblom, W. Shi, P. Huang, L. Eriksson, H. Weihe, S. Styring, B. Åkermark, R. Lomoth, and A. Magnuson, Eur. J. Inorg. Chem. **2006**, 5033 (2006).
- ⁷Z. Chen, J. J. Concepcion, H. Luo, J. F. Hull, A. Paul, and T. J. Meyer, J. Am. Chem. Soc. **132**, 17670 (2010).
- ⁸T. H. Parsell, M.-Y. Yang, and A. S. Borovik, J. Am. Chem. Soc. **131**, 2762 (2009).
- ⁹C. Ohde and C. Limberg, Chem. Eur. J. 16, 6892 (2010).
- ¹⁰ X. Ribas, C. Calle, A. Poater, A. Casitas, L. Gómez, R. Xifra, T. Parella, J. Benet-Buchholz, A. Schweiger, and G. Mitrikas, J. Am. Chem. Soc. 132, 12299 (2010).
- ¹¹C. Chatgilialoglu, M. D'Angelantonio, P. Kaloudis, Q. G. Mulazzani, and M. Guerra, J. Phys. Chem. Lett. 1, 174 (2010).
- ¹²G. J. Christian, A. Llobet, and F. Maseras, Inorg. Chem. 49, 5977 (2010).

- ¹³S. Y. Reece, J. M. Hodgkiss, J. Stubbe, and D. G. Nocera, Philos. Trans. R. Soc., B 361, 1351 (2006).
- ¹⁴B. H. Solis, A. G. Maher, D. K. Dogutan, D. G. Nocera, and S. Hammes-Schiffer, Proc. Natl. Acad. Sci. U. S. A. 113, 485 (2016).
- ¹⁵P. Li, A. V. Soudackov, and S. Hammes-Schiffer, J. Am. Chem. Soc. **140**, 3068 (2018).
- ¹⁶E. R. Sayfutyarova, Z. K. Goldsmith, and S. Hammes-Schiffer, J. Am. Chem. Soc. 140, 15641 (2018).
- ¹⁷T. Irebo, S. Y. Reece, M. Sjödin, D. G. Nocera, and L. Hammarström, J. Am. Chem. Soc. **129**, 15462 (2007).
- ¹⁸T. F. Markle, I. J. Rhile, A. G. DiPasquale, and J. M. Mayer, Proc. Natl. Acad. Sci. U. S. A. **105**, 8185 (2008).
- ¹⁹ M. T. Huynh, S. J. Mora, M. Villalba, M. E. Tejeda-Ferrari, P. A. Liddell, B. R. Cherry, A.-L. Teillout, C. W. Machan, C. P. Kubiak, D. Gust, T. A. Moore, S. Hammes-Schiffer, and A. L. Moore, ACS Cent. Sci. 3, 372 (2017).
- ²⁰C. J. Gagliardi, L. Wang, P. Dongare, M. K. Brennaman, J. M. Papanikolas, T. J. Meyer, and D. W. Thompson, Proc. Natl. Acad. Sci. U. S. A. 113, 11106 (2016).
- ²¹ C. V. Pagba, T. G. McCaslin, S.-H. Chi, J. W. Perry, and B. A. Barry, J. Phys. Chem. B 120, 1259 (2016).
- ²² A. Pannwitz and O. S. Wenger, J. Am. Chem. Soc. **139**, 13308 (2017).
- ²³S. V. Lymar, M. Z. Ertem, A. Lewandowska-Andralojc, and D. E. Polyansky, J. Phys. Chem. Lett. 8, 4043 (2017).
- ²⁴ A. Migliore, N. F. Polizzi, M. J. Therien, and D. N. Beratan, Chem. Rev. 114, 3381 (2014).
- ²⁵S. Y. Reece and D. G. Nocera, Annu. Rev. Biochem. **78**, 673 (2009).
- ²⁶ M.-T. Zhang, T. Irebo, O. Johansson, and L. Hammarström, J. Am. Chem. Soc. 133, 13224 (2011).
- ²⁷T. F. Markle, M.-T. Zhang, M.-P. Santoni, L. O. Johannissen, and L. Hammarström, J. Phys. Chem. B 120, 9308 (2016).
- ²⁸S. D. Glover, G. A. Parada, T. F. Markle, S. Ott, and L. Hammarström, J. Am. Chem. Soc. **139**, 2090 (2017).
- ²⁹L. O. Johannissen, T. Irebo, M. Sjödin, O. Johansson, and L. Hammarström, J. Phys. Chem. B **113**, 16214 (2009).
- ³⁰S. Hay and N. S. Scrutton, Nat. Chem. **4**, 161 (2012).
- ³¹ J. P. Layfield and S. Hammes-Schiffer, Chem. Rev. **114**, 3466 (2014).
- ³²G. F. Manbeck, E. Fujita, and J. J. Concepcion, J. Am. Chem. Soc. **138**, 11536 (2016).
- ³³Y. Yoneda, S. J. Mora, J. Shee, B. L. Wadsworth, E. A. Arsenault, D. Hait, G. Kodis, D. Gust, G. F. Moore, and A. L. Moore, J. Am. Chem. Soc. 143, 3104 (2021)
- 34 L. Chen and J. A. Fournier, J. Phys. Chem. A 125, 9288 (2021).
- 35 L. Chen, J. L. S. Dean, and J. A. Fournier, J. Phys. Chem. A 125, 10235 (2021).
- ³⁶M. Frisch, G. W. Trucks, H. B. Schlegel, G. E. Scuseria, M. A. Robb, J. R. Cheeseman, G. Scalmani, V. Barone, B. Mennucci, and G. Petersson, Gaussian 09, Gaussian, Inc., Wallingford, CT, 2009.
- ³⁷S. M. Craig, F. S. Menges, C. H. Duong, J. K. Denton, L. R. Madison, A. B. McCoy, and M. A. Johnson, Proc. Natl. Acad. Sci. U. S. A. 114, E4706 (2017).
- ³⁸R. M. Badger, J. Chem. Phys. **2**, 128 (1934).
- ³⁹ M. Charton, Prog. Phys. Org. Chem. **8**, 235 (1971).
- $^{\bf 40}$ A. E. Habboush and S. J. S. Al-Bazi, J. Chromatogr. Sci. 16, 296 (1978).
- ⁴¹ P. Segura, J. Org. Chem. **50**, 1045 (1985).
- ⁴²C. J. Johnson, L. C. Dzugan, A. B. Wolk, C. M. Leavitt, J. A. Fournier, A. B. McCoy, and M. A. Johnson, J. Phys. Chem. A 118, 7590 (2014).
- ⁴³C. T. Wolke, A. F. DeBlase, C. M. Leavitt, A. B. McCoy, and M. A. Johnson, J. Phys. Chem. A 119, 13018 (2015).
- ⁴⁴ A. F. DeBlase, S. Bloom, T. Lectka, K. D. Jordan, A. B. McCoy, and M. A. Johnson, J. Chem. Phys. **139**, 024301 (2013).
- ⁴⁵W. H. Robertson, E. A. Price, J. M. Weber, J.-W. Shin, G. H. Weddle, and M. A. Johnson, J. Phys. Chem. A **107**, 6527 (2003).
- ⁴⁶E. M. Myshakin, K. D. Jordan, E. L. Sibert III, and M. A. Johnson, J. Chem. Phys. 119, 10138 (2003).

⁴⁷ N. Heine, E. G. Kratz, R. Bergmann, D. P. Schofield, K. R. Asmis, K. D. Jordan, and A. B. McCoy, J. Phys. Chem. A **118**, 8188 (2014).

⁴⁸ A. V. Zabuga, M. Z. Kamrath, and T. R. Rizzo, J. Phys. Chem. A **119**, 10494 (2015).

⁴⁹P. Hamm and G. Stock, J. Chem. Phys. **143**, 134308 (2015).

⁵⁰ N. Yang, C. H. Duong, P. J. Kelleher, and M. A. Johnson, Nat. Chem. **12**, 159 (2020).

⁵¹E. L. Sibert, K. N. Blodgett, and T. S. Zwier, J. Phys. Chem. A 125, 7318 (2021).

⁵² M. Balasubramanian, A. Reynolds, T. J. Blair, and M. Khalil, Chem. Phys. 519, 38 (2019).

⁵³ A. B. McCoy, T. L. Guasco, C. M. Leavitt, S. G. Olesen, and M. A. Johnson, Phys. Chem. Chem. Phys. **14**, 7205 (2012).

⁵⁴M. A. Boyer and A. B. McCoy, J. Chem. Phys. **156**, 054107 (2022).